



# 1 A New Approach for Rainfall Rate Field Space-Time Interpolation for 2 Western Europe

3  
4 Guangguang Yang<sup>1</sup>, David Ndzi<sup>2</sup>, Kevin Paulson<sup>3</sup>, Misha Filip<sup>1</sup>

5 <sup>1</sup>School of Engineering, University of Portsmouth, Portsmouth, PO1 3DJ, United Kingdom

6 <sup>2</sup>School of Engineering, University of West of Scotland, Paisley, United Kingdom

7 <sup>3</sup>School of Engineering, University of Hull, Hull, HU6 7RX, United Kingdom

8 [guangguang.yang@myport.ac.uk](mailto:guangguang.yang@myport.ac.uk); [david.ndzi@uws.ac.uk](mailto:david.ndzi@uws.ac.uk); [K.Paulson@hull.ac.uk](mailto:K.Paulson@hull.ac.uk); [misha.filip@port.ac.uk](mailto:misha.filip@port.ac.uk)

9

10 **Abstract.** The prediction of rainfall rate characteristics at small space-time scales is currently an important topic, particularly within the context  
11 of the planning and design of satellite network systems. A new comprehensive interpolation approach is presented in this paper to deal with  
12 such an issue. There are three novelties in the proposed approach: 1) the proposed interpolation approach is not directly applied to measured  
13 rain precipitation (either radar or raingauge-derived data) but focuses on the coefficients of the fitted statistical distributions and/or computed  
14 rain characteristics at each location; 2) the parameter databases are provided and the contour maps of coefficients spanning Western Europe  
15 have been created. It conveniently and efficiently provides the rain parameter for any location within the studied map; 3) more speculatively,  
16 the 3D space-time interpolation approach can extrapolate to rain parameters at space-time resolutions shorter than those in the NIMROD  
17 databases.

## 18 1. Introduction

19 The spatial and temporal variation of point rainfall rates is important for the detailed planning and performance prediction for  
20 satellite and terrestrial networks (a group of links) (Yang, 2016). It is increasingly evident that models and/or approaches are  
21 needed in order to predict rainfall rate variation at smaller space-time scales than currently available from wide area coverage  
22 measured rainfall rate databases.

23 Extensive studies of rain have been carried out in the last few decades. After several generations many interesting rain models  
24 have been published. A model of particular interest was developed by Bell (Bell, 1987). His work showed that rainfall intensities  
25 in a field exhibit lognormal distribution and this was confirmed by Crane (Crane, 1996) and Jeannin et al (Jeannin et al., 2008).  
26 The traditional rain models (e.g. stochastic models, Markov chain models) can be used to aid the planning of satellite networks.  
27 However, there are some limitations inherent in such models and the two major ones are:

- 28 1) Data availability. The models are only applicable to areas/locations where rainfall precipitation with the necessary  
29 integration volume has been observed and the accuracy of the models in areas where no data is available is difficult to verify.
- 30 2) Integration volume. The application of the traditional models is limited by the integration length. The modelling of rain and  
31 simulated rainfall fields can only be limited to the space-time resolution derived from rain radar/gauge measurements.  
32 Rainfall fields simulation at finer space-time scales is often possible but cannot be verified.

33 Based on this information, it is clear that the application range of stochastic models is limited by the above problems.  
34 Improvements, thus, are needed to compensate, enhance and extend the performance of stochastic models. In particular, an  
35 increase in the use of high frequency over short communication links has led to an increase in the need to predict rainfall rates at  
36 finer resolutions. Current stochastic models cannot satisfy this demand. As a result, interpolation techniques have attracted a lot  
37 of attention in recent decades. For example, Drozdov and Sephelevskii (Drozdov and Shepelevskii, 1946) developed a spatial  
38 interpolation technique to analyze the spatial variations of a process over an area. Then later, a modified interpolation technique



39 called Kriging was developed based on the theory of regionalized variables to estimate area averages considered as realizations  
40 of a stochastic process introduced by Matheron (Matheron, 1971) Since then significant progress has been made and two-  
41 dimensional ( $2D$ ) space rainfall rate interpolation models have been developed, e.g.(Deidda,1999 and Menabde et al., 1997). The  
42 Random Midpoint Displacement algorithm (RMD) developed by Voss (Voss, 1985) in 1985 is one of the most popular  
43 interpolation algorithms. The basic idea of the technique is to introduce new rain rate samples with the same underlying  
44 distribution as existing measurements at new locations or times. The one-dimensional ( $1D$ ) time interpolation is also of interest  
45 as network planners and designers of physical layer fade mitigation techniques (Gremont et al., 1999) require knowledge of rain  
46 variation over much shorter time scales (of the order of seconds or less). Some excellent models have been published like  
47 (Pathirana et al., 2003 and Veneziano et al., 1996). One of such models proposed by Kevin Paulson (Paulson, 2004) is a  
48 stochastic numerical model that can interpolate the point rain rate for short time durations down to 10 s.

49 The downscaling model, based on the space-time averaging theory, is another model that has also attracted significant attention.  
50 According to (Deidda et al., 1999), there are two fundamental requirements for precipitation downscaling models, which are: 1)  
51 understanding of the statistical properties and scaling laws of rainfall fields, and 2) validation of downscaling models that are  
52 able to preserve statistical characteristics observed in real precipitation. Typically, based on the information given in (Rebora et  
53 al., 2006), downscaling algorithms can generally be grouped into three main families with some simplification: 1) point process  
54 based on the random positioning of a given number of rain bands and rain cells (Cowpertwait et al., 2006); 2) autoregressive  
55 processes passed through a static nonlinear transformation (Guillot and Lebel, 1999), and; 3) fractal cascades (Kiely and  
56 Ivanova, 1999). In particular, the theory of fractals, which was first introduced by Mandelbrot in 1967 (Mandelbrot, 1967) has  
57 attracted great attention. This theory was not applied to rainfall study until the mid-1980s (Lovejoy and Mandelbrot, 1985). Rain  
58 has been shown to hold fractal properties over a range of scales. The intermittence and discontinuous nature of rain is reproduced  
59 by the fractal based models, which are strongly favoured for rainfall modelling. Many studies have been carried out to interpolate  
60 the radar/raingauge measurement data to finer scales using the fractal theory, such as (Svensson, 1996). Multifractal models,  
61 which may be simulated using random cascades, can easily capture any moment of the observed signal; especially higher order  
62 moments have attracted a lot of attention. Because of their link with multifractal theory, multiplicative cascade models first  
63 proposed by Yaglom (Yaglom, Jul 1966), appeal to rainfall simuláations. The rainfall series have been shown to exhibit scaling  
64 invariance properties over a large range of space (Olsson, 1996) and time (Olsson et al., 1993) steps. Some multifractal models  
65 use discrete cascade algorithms to produce data at finer scales from original sparse observations, for example (Olsson, 1998). A  
66 classic work is given by Menabde (Menabde, 1997) who used a discrete random cascade to generate a rain field with the desired  
67 statistical structure and then applied a power law filter, thereby removing some of the blockiness resulting in a more realistic  
68 looking rain field. In addition, synthesis of rain field at high resolution is also important to the rain study especially devised for  
69 applications related to EM wave propagation. Many contributions have been done in this area, such as (Jeannin, 2012 and Luini,  
70 2011)

71 The prediction at finer space-time resolution however, has long been a challenging issue in rainfall field modeling. Results from  
72  $3D$  interpolation studies are quite poor (Yang, 2016 and Deidda, 2000) as it is very difficult to consider both space and time  
73 variability and irregularity of rainfall in an appropriate way. The basic idea of published models is to try to find the underlying  
74 principle of how the space-time transformation can be achieved. A representative model was developed by Deidda (Deidda,  
75 2000) based on the assumption that Taylor's hypothesis (Taylor, 1938) can be applied. The space-time rainfall field is assumed  
76 to be a three-dimensional ( $2D$  space and  $1D$  time) homogeneous and isotropic process. An advection velocity parameter is  
77 introduced to connect the space scale and time scale. With the help of a velocity parameter, the statistical properties of rain at  
78 finer scales can be deduced from larger ones. Similar studies can be found in (Venugopal et al, 1999, Deidda, 2006 and



79 Venugopal et al., 1999) in which rain has been studied in a range of space-time scales to define the transformation parameter. In  
80 particular, Kundu and Bell (Kundu and Bell, 2006) developed a model that can provide the correlation function of rain in 3D  
81 space-time domain but in a very complicated form.

82 The absence of high resolution rainfall data at desired space and time scales is the main knowledge gap. Deidda in (Deidda,  
83 2000) pointed out that most of the existing rainfall studies at finer scales are purely focused on either space modeling (Hubert et  
84 al., 1993) or time modeling (Paulson, 2004). However, both of these approaches have limitations. For example, the statistical  
85 behavior of rain in time has implicit consideration of the spatial distribution and extension of the rain field itself; and the study in  
86 space is normally based on fixed time duration whilst the evolution in time of spatial patterns is ignored. Accurate rainfall field  
87 simulation requires knowledge of rainfall rate variability in both space and time domains. There is not enough research in the  
88 area of space-time interpolation apart from a few works, such as (Deidda, 2006). Thus, an appropriate space-time interpolation  
89 model that can preserve the underlying statistical properties at finer scales is needed. The absence of knowledge of rain  
90 characteristics at high space and time resolution is another important gap and is the second objective of this study. Kundu in  
91 (Kundu and Bell, 2006) showed that the characteristics of rain depend on the space and time scales over which rain data is  
92 averaged. However, all the existing interpolation and/or multifractal models directly focus on rain precipitation and no work has  
93 been found that studied the characteristics of rain at scales better than the one provided by rain radars. The study in this paper,  
94 therefore, will look into this issue to investigate the variability of rain characteristics at arbitrary space-time integration length.

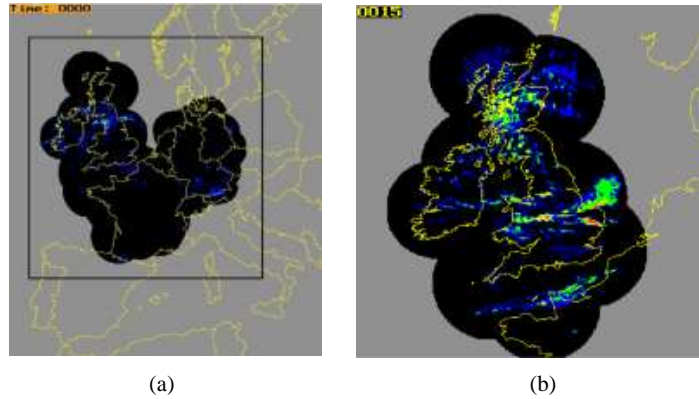
95 To further the development of rain-induced radio-wave attenuation models, and to provide more accurate performance prediction  
96 of satellite links over wide areas, there is an increasing need for a good understanding of the space-time characteristics of rainfall  
97 rate at finer scales. As extension of our previous work (Yang, 2011), this paper presents a simple but accurate space-time  
98 interpolation approach that can interpolate the key studied properties of rain in both space and time domain simultaneously. We  
99 present a series of European maps superimposed with each parameter at different space-time resolution which is novel. In  
100 particular, a simple but accurate approach for interpolating the rain characteristics has been proposed. It can predict the  
101 coefficient values of the statistical model in both space and time with reasonable accuracy.

102 The rest of this paper is organized as follows: Section 2 describes the data used in this study. Section 3 reviews the statistical  
103 model proposed in previous work and describes the proposed approach how to interpolate the measurements into 3-dimensional  
104 space-time domain. The detailed results, including the 2D contour map of rain characteristics across Western Europe, as well as  
105 the 3D space-time predictions at each location, are presented in Section 4. Section 5 validates the results achieved from the  
106 proposed interpolation approach. Conclusions are drawn in Section 6.

## 107 2. Data Description

108 Five complete years of NIMROD rain radar data (from 2005 to 2009) have been analyzed for the development of a generic  
109 interpolation approach. The NIMROD radar system produces a series of composite rain field map by every 15 mins. The  
110 measured rain rate samples are distributed on a 5 km squared Cartesian grid covering Western Europe. Each NIMROD map  
111 contains 700 × 620 data cells, but only the data available points have been analysed, see the outline is Fig. 1(a). The study area  
112 ranges from 43.1938° to 59.4306° in latitude and -9.7370° to 19.8364° in longitude. In addition, NIMROD system also holds  
113 the database for the British Isles. This database has better resolution of rain rate measurement, which is 1 km in space and  
114 5 mins in time. The example radar map is given in Fig. 1(b). The performance of any model or approach needs to be validated  
115 through comparing with observational data from apparatus (e.g. raingauge or rain radar). UK data, which has better resolution  
116 than EU NIMROD data, can be utilized to implement the validation.

117



118  
 119

120 **Figure 1:** (a) composite radar scan image: radar image for Western Europe (the outline is the studied area), and (b) radar image  
 121 for the British Isles.

### 122 3. Methodology

#### 123 3.1. Stochastic Model

124 The empirical equations that can accurately provide the estimates of the studied characteristics of rain have been discussed in 0.  
 125 The proposed model for the four key rain characteristics is described briefly here for completeness.

126 It is well accepted that rainfall rate  $R$  in mm/h at one location is modeled as a lognormal process with mixed probability density  
 127 function (pdf). According to (Filip and Vilar, 1990), the general formula for a straight line fit is given by:

$$128 Q_{inv} = \frac{\ln(R)}{\sigma} + \frac{\mu}{\sigma} \quad (1)$$

129 where  $\{\mu, \sigma\}$  is the set of lognormal parameters that are used to study the statistics of rainfall rate at a location of interest.  
 130 Research reported in (Yang, 2016) has produced a single general empirical equation that fits both the space correlation and the  
 131 time correlation functions. The common function is given by:

$$132 \rho(x) = \frac{a}{a+x^n} \quad (2)$$

133 where  $x$  can either be  $d$  which represents the distance in *km* or  $t$  which is the time lag in *mins*.

134 An empirical equation has been proposed in (Yang, 2011) that can give an excellent estimate of the probability of rain  
 135 occurrence ( $P_0$ ) throughout the whole range of integration length. The mathematical equation is described by:

$$136 P_0(x) = 100 - b \exp(cx^e) \quad (3)$$

137 where  $b$ ,  $c$  and  $e$  are experimental constants which can be determined from study and  $x$  denotes either spatial integration length  $L$   
 138 or temporal integration length  $T$ .

#### 139 3.2. Data Integration

140 Following previous work (Yang, Oct 2011), the rainfall rate data can be up-scaled from short integration length to longer  
 141 one using:

$$142 R_\lambda(x, y, t) = \frac{1}{\lambda^3 \varphi^2 T} \int \int \int R(x', y', t') I\left(\frac{x-x'}{\lambda L}, \frac{y-y'}{\lambda L}, \frac{t-t'}{\lambda T}\right) dx' dy' dt' \quad (4)$$

143 where  $R_\lambda(x, y, t)$  is the rain rate at position  $(x, y)$  derived from a spatial integration region of linear size  $\lambda L$  and temporal  
 144 integration time  $\lambda T$ .  $\lambda > 1$  is known as the scale parameter. More generally, the spatial and temporal regions could have  
 145 different scale parameters e.g.:

$$147 R_\lambda(x, y, t) = \frac{1}{\lambda^2 \varphi^2 T} \int \int \int R(x', y', t') I\left(\frac{x-x'}{\lambda L}, \frac{y-y'}{\lambda L}, \frac{t-t'}{\varphi T}\right) dx' dy' dt' \quad (5)$$

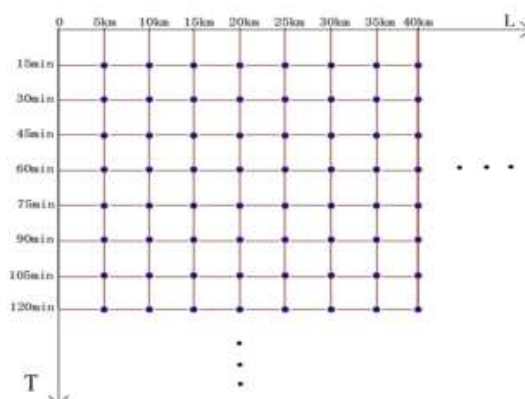


148 The radar-derived rain rate data can be upscaled to coarser resolution based on above equations. It is important to highlight that  
149 each grid point will be used only once for each integration and no overlapping regions are considered. The integrated data will be  
150 tiled up without changing the size of original rain map but new dataset with larger integration scale will be achieved. Note that  
151 the larger the integration length the smaller number of data samples will be. Particularly, it requires  $\lambda$  and  $\varphi$  must be integer to  
152 enable this procedure. Therefore, it is notable that the integration length of the new data is the integral times of original radar  
153 data, and it will be  $\lambda L$  and  $\varphi T$ , here  $L = 5 \text{ km}$  and  $T = 15 \text{ mins}$ .

### 154 3.3. Approach for the Implementation of 3D Interpolation

155 According to our previous work (Yang, 2011), we found that the rain characteristics regularly changing with increasing  
156 integration length both in space and time domains. This interesting finding indicates that the studied rain characteristics at other  
157 spatial or temporal integration lengths can be reasonably predicted using such regularity. More speculatively, it enables the 3D  
158 interpolation to be achievable if there are enough measurements with different space-time resolution combinations.

159 Fig.2 shows the grid of available rain data points from the NIMROD radar measurements. The dots represent the available space-time  
160 time integration length combination where the rain characteristics can be computed based on available NIMROD data. The lines  
161 represent the range of integration length where rain characteristics can be calculated from equation (1) to (3). It is notable that the  
162 proposed statistical model in our previous work can only produce estimation of rain characteristics along the line but not the  
163 blank area. Taking advantage of the regular distribution of the measurements, the key rain characteristics at other spatial-  
164 temporal integration lengths can be predicted using any existing interpolation technique.



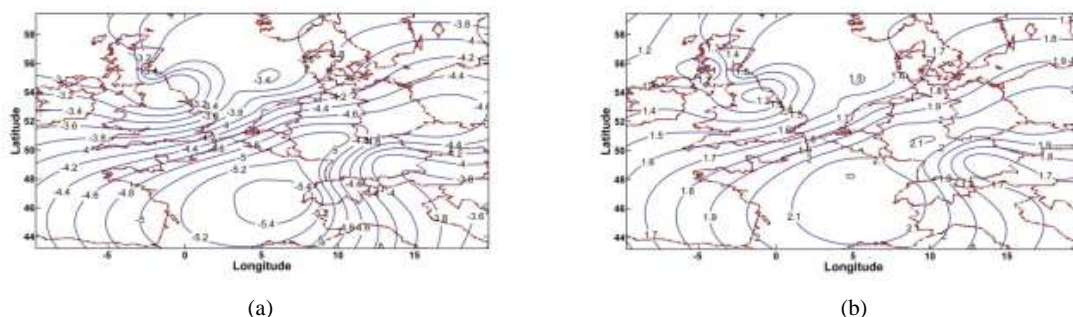
165

166 **Figure 2:** Grid of available rain data points from the NIMROD radar measurements. The dots represent the available space-time  
167 integration length combination where the rain characteristics can be computed based on available NIMROD data.

## 168 4. Experimental Results

### 169 4.1. Contour Map of Rain Characteristics

170 The proposed statistical model can provide estimates of key rain characteristics (including the first order statistics of rain, the  
171 spatial and temporal correlation of rain rate, as well as the probability of rain/no rain) in two dimensions. Considerable  
172 computation is required to extract these summarizing statistics from the NIMROD databases. Based on the proposed model,  
173 however, the rain characteristics at any data available locations within the Western Europe can be achieved. The work in this  
174 paper has produced a multi-resolution database of parameters and contour maps that cover the whole of Western Europe. With  
175 the help of this database, the user can easily obtain the characteristics of rain (or the distribution coefficients) at any location  
176 within the studied area.



177  
 178

179 **Figure 3:** Contour maps of rain distribution coefficients with spatial integration length of 5 km and temporal integration length  
 180 15 min: (a) a plot of  $\mu$  values and (b) a plot of  $\sigma$  values.

181 Example contour maps of the log-Normal rain rate distribution parameters  $\{\mu, \sigma\}$  are presented in Fig. 3. Here, the longitude and  
 182 latitude values are achieved by using the approach given in Appendix A. Fig. 3(a) is the map of  $\mu$  values cross the Western  
 183 Europe and Fig. 3(b) is  $\sigma$  values. The background is the map of the Western European coastline, and the calculated parameter at  
 184 each individual location (here the spatial integration length is 5 km and the temporal integration length is 15 mins) is  
 185 superimposed on the map. It shows that the contour map can provide the parameter value at any location within the range from  
 186  $-9.7370^\circ$  to  $19.8364^\circ$  in longitude and between  $43.1938^\circ$  to  $59.4306^\circ$  in latitude. The calculated values are stored in a database  
 187 from which  $\{\mu, \sigma\}$  can be easily obtained by simply inputting the longitude and latitude information for any desired location. This  
 188 is very convenient as almost no computation time is needed. Similar results of other rain characteristics have also been produced  
 189 and stored in the database, but not presented in this paper. In addition, the rain characteristics at other integration length  
 190 combinations between  $\{5 \text{ km}, 15 \text{ mins}\}$  and  $\{75 \text{ km}, 120 \text{ mins}\}$  have been computed and stored in the database. Given this  
 191 database, the prediction of the rain characteristics at some finer space-time resolutions can be estimated by interpolation.

#### 192 4.2. Prediction of Rain Characteristics in Space-Time

193 The existing NIMROD radar maps have been integrated to some integration length combinations from  $\{5 \text{ km}, 15 \text{ mins}\}$  to  
 194  $\{75 \text{ km}, 120 \text{ mins}\}$ . The key characteristics of rain were then analysed to see how they vary with integration length. Table 1  
 195 gives an example of the probability of rain ( $P_0$ ) with a range of integration length combinations, at Portsmouth (UK).

196

197 **Table 1:** Probability of rain occurrence for increasing spatial-temporal integration lengths ranging from 5 km to 75 km and  
 198 15 mins to 120 mins at Portsmouth.

$L$	$T$							
	15 mins	30 mins	45 mins	60 mins	75 mins	90 mins	105 mins	120 mins
5 km	15.0	22.9	25.9	28.5	30.5	32.6	34.3	36.1
10 km	23.4	28.61	32.3	35.3	37.7	40.1	41.9	43.8
15 km	28.6	33.7	37.5	40.3	42.9	44.9	46.7	48.6
20 km	32.6	37.9	41.6	44.7	47.1	49.4	51.4	53.1
25 km	35.2	40.6	44.1	47.2	49.5	51.7	53.7	55.2
35 km	42.5	48.3	52.2	55.4	57.9	60.1	61.2	63.1
40 km	45.9	49.4	53.2	56.1	59.6	62.6	64.4	67.9
45 km	48.8	55.6	59.5	62.2	64.7	66.6	68.2	69.6
50 km	49.9	56.2	60.2	62.9	65.6	67.2	69.5	71.8
55 km	56.5	62.2	65.8	68.5	70.7	72.2	73.5	75.3
65 km	60.9	65.5	68.5	70.6	72.3	74.2	75.1	76.5
75 km	63.9	69.1	72.4	74.4	76.3	77.8	78.7	79.9



199 It shows that the  $P_0$  value changes with increasing spatial-temporal integration length. Similar results can be found for other  
 200 studied parameters. These data allow the prediction of parameters at other space-time resolutions. The top-left hand corner of the  
 201 table is the computed value with the shortest available spatial-temporal integration length ( $\{5 \text{ km}, 15 \text{ mins}\}$ ) derived from EU  
 202 NIMROD radar, and the right-hand bottom corner is the coarsest one ( $\{75 \text{ km}, 120 \text{ mins}\}$ ) after integration. From Table 1, one  
 203 can see that the characteristics of rain change systematically with increasing integration length. Given this finding the predictions  
 204 at finer resolution can be estimated by interpolation.

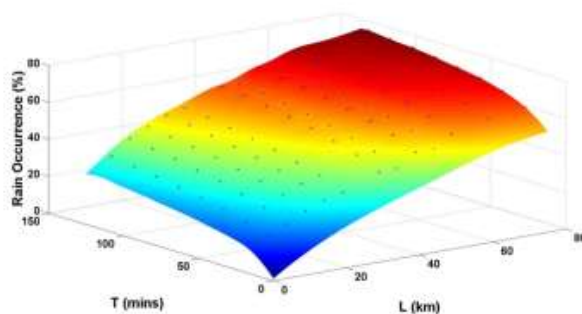
205 In this study, the cubic spline interpolation algorithm has been chosen to implement this task. The cubic spline is a function that  
 206 is constructed by piecing together cubic polynomial on different intervals (Keys, 1981). It has the form

$$207 \quad S(x) = \begin{cases} s_1(x) & \text{if } x_1 \leq x < x_2 \\ s_2(x) & \text{if } x_2 \leq x < x_3 \\ \dots & \dots \\ s_{n-1}(x) & \text{if } x_{n-1} \leq x < x_n \end{cases} \quad (6)$$

208 where  $s_i$  is a third degree polynomial defined by:

$$209 \quad s_i(x) = a_i(x - x_i)^3 + b_i(x - x_i)^2 + c_i(x - x_i) + d_i \quad (7)$$

210  
 211 Cubic spline is often used for 1D interpolation. The data in each row and column of the database (see the example in Table 1)  
 212 can be treated as samples in one dimension. It enables the use of cubic spline interpolation to estimate parameter values at other  
 213 scales, based on the measured parameters. The first step is to extract the multi-scale parameters for a desired location from the  
 214 database. Cubic spline interpolation is then used to interpolate to a different spatial or temporal integration sizes. In this study,  
 215 the “bicubic” interpolation algorithm in MATLAB was used. Mathematically, the bicubic interpolation, which is an extension of  
 216 1D cubic interpolation, is used to interpolate data points on a two dimensional regular grid. It can be accomplished using cubic  
 217 spline algorithm (we provide part of the software program in Appendix B to show the approach of 3D space-time interpolation).  
 218 The software proposed in this work uses the produced parameters’ database. It contains the fitted rain parameters for a range of  
 219 integration lengths between  $\{5 \text{ km}, 15 \text{ mins}\}$  and  $\{75 \text{ km}, 120 \text{ mins}\}$  for the whole of the studied area (Western Europe). The  
 220 software extracts the rain characteristics with all available integration lengths at the location of interest. Taking the extracted data  
 221 as input values, the interpolation algorithm then processes the data and gives the prediction at other space-time resolutions. Note  
 222 that this is true only for the locations for which radar measurements data is available (the black area in Fig. 1).



223

224

**Figure 4:** An example of 3D space-time interpolation of  $P_0$  at Portsmouth.

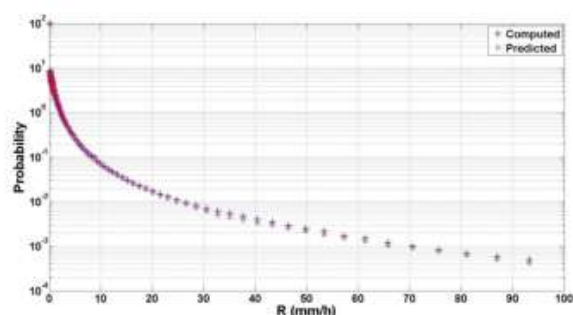
225 Fig. 4 presents the example of predicted probability of rain occurrence at other spatial-temporal integration lengths, along with  
 226 the measured data in Table 1, for Portsmouth. It is clear that the outcome of the 3D interpolation is a surface constructed from  
 227 many 2D curves both in space and time domains. The dots are the measured values at a range of spatial-temporal integration  
 228 lengths that are multiples of the data resolution, whilst the surface is produced by the interpolation algorithms to be consistent



229 with these data. The multi-scale data are regularly spaced, which reduces the complexity of the interpolation algorithm.  
230 Interestingly, the results show that  $P_0$  values increase systematically with increasing spatial-temporal integration length. In  
231 addition, by interpolation the values at resolutions smaller than  $\{5 \text{ km}, 15 \text{ mins}\}$  can also be predicted. The extrapolation can be  
232 constrained by the assumption that  $P_0 \rightarrow 0$  as either  $\lambda \rightarrow 0$  or  $\varphi \rightarrow 0$ . This enables the predictions to be plotted smoothly to form  
233 a 3D surface. The resolution of the studied key characteristics of rain offers significant improvements over previous methods  
234 (e.g. Bell, 1987) and it is these that are important for rainfall field simulation studies in future. The salient point of the proposed  
235 interpolation approach is that the best estimate can be obtained with high accuracy for the space and time resolutions up to 50m  
236 and 6s, respectively. Predictions finer than this threshold are unacceptable as negative data is produced. This is impossible due to  
237 the  $P_0$  should not less than 0. Other interpolation technique might give better results but this is not covered in this paper. The  
238 validity of the interpolated parameters needs to be tested, and this is limited by the availability of data at small spatial and  
239 temporal integration volumes. One test that can be performed is to use  $\{5 \text{ km}, 15 \text{ mins}\}$  EU NIMROD data to predict the  
240 distribution and correlation functions of  $\{1 \text{ km}, 5 \text{ mins}\}$  UK NIMROD data.

## 241 5. Validation

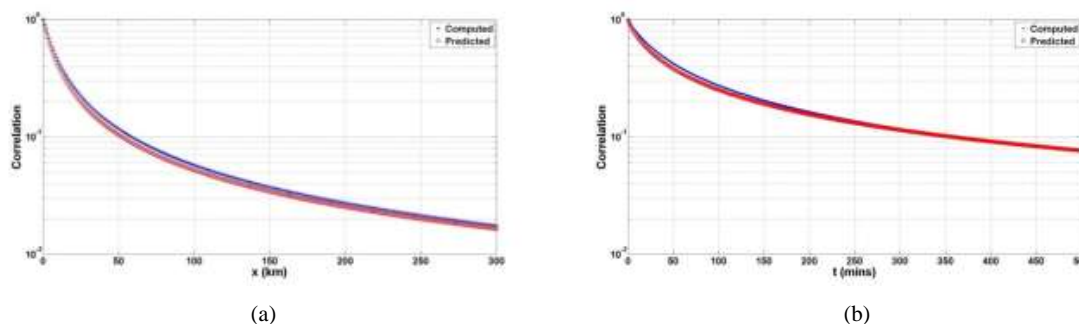
242 The absence of measured data at the smaller space-time scales causes great difficulties in validating the proposed method.  
243 However, the  $\{1 \text{ km}, 5 \text{ mins}\}$  UK NIMROD radar measurements can be used to address this issue to some extent. In this paper,  
244 the key rain characteristics at Portsmouth have been estimated at scales of  $\{1 \text{ km}, 5 \text{ mins}\}$  and these were compared with  
245 interpolations from the EU NIMROD data.



246  
247 **Figure 5:** A comparison exceedance distribution of rainfall rate estimated by interpolation from 5 km data to 1 km data and  
248 estimated directly for 1 km data.

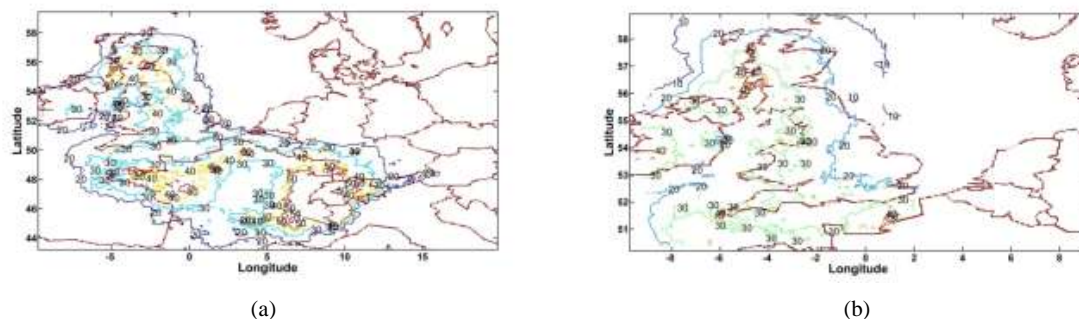
249 Fig. 5-6 present comparisons of rainfall rate characteristics estimated by extrapolation from 5 km EU NIMROD to 1 km data  
250 and estimated directly from 1 km UK NIMROD data. The predicted  $\{\mu, \sigma\}$  values are  $\{-3.75, 2.12\}$  and the computed values  
251 are  $\{-3.85, 2.04\}$ . The predicted probability of rain occurrence ( $P_0$ ) and measured one are 12.5% and 12.1%, respectively.  
252 Although the  $\{\mu, \sigma, P_0\}$  values of both are marginally different (2.7%, 3.8%, 2.7% differences for  $\mu, \sigma, P_0$ , respectively), the  
253 associated 0.1%, 0.01% and 0.001% exceeded rain rates are similar, this can be seen in Fig. 5. In particular, the proposed model  
254 gives excellent approximation for the first-order rainfall rate statistics, especially for the rain rate lower than 40 mm/h for which  
255 the accuracy is higher than 90%. The probability of heavy rain event is extremely low so that there is no sufficient data is  
256 available. This results in the higher bias for the range where  $R > 40 \text{ mm/h}$ . Fig. 6(a) shows that the spatial correlation using the  
257 predicted values is in agreement with the computed values. There is a small difference between the temporal correlation  
258 functions of rain rate using predicted data and measured data at short time lags up to roughly 150 mins, see Fig. 6(b). However,  
259 the result is still acceptable as the trend is similar, especially for large time lags. This shows that the approach proposed in this

260 paper has potential and requires considerable less computational effort than the direct estimation of these distributions from the  
261 data. However, the rain characteristics at scales finer than  $\{1 \text{ km}, 5 \text{ mins}\}$  cannot be validated due to lack of radar/raingauge  
262 data.



263  
264

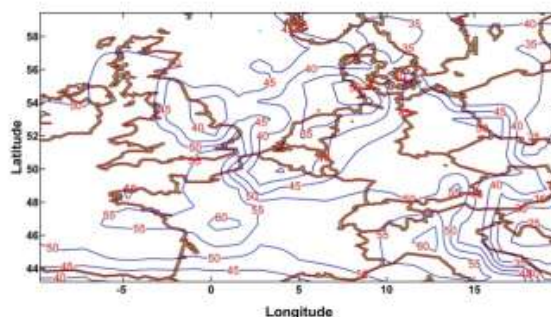
265 **Figure 6:** A comparison of correlation function of rainfall rate estimated by interpolation from 5 km data to 1 km data and  
266 estimated directly for 1 km data: a) spatial correlation function; b) temporal correlation function.



267  
268

269 **Figure 7:** Contour map of 0.01% exceeded rain rates: a) predicted by interpolation from 5 km EU NIMROD to 1 km; b)  
270 measured from 1 km UK NIMROD.

271  
272 Fig. 7(a) shows the map of 0.01% exceeded rain rates across the Western Europe predicted by interpolation from the 5 km EU  
273 NIMROD to 1 km. The results are plausible for most areas. However, it shows that radars accuracy is affected in the Grand  
274 Massive alpine area of France. Fig. 7(b) presents the map of 0.01% exceeded rain rates across the British Isles given by the  
275 1 km UK NIROMD. Note that the rain rate with 0.01% exceedance in both figures tends to reduce towards the edge of the radar  
276 region and this is almost certainly an artefact. It could be due to how the contour function deals with NaN (caused by data  
277 unavailable); or something to do with the data at the edge of the radar network. The contour map of 0.01% exceeded rain rate of  
278 the average year given by ITU-R P 837-6 (ITU, 2013) is presented in Fig. 8. These two figures (Fig. 7 and Fig. 8), illustrate that  
279 the results of the statistics in Fig. 7 are very similar. This indicates that the proposed model can give a reasonable estimation of  
280 rain parameters that can be used to produce rain rates with 0.01% exceedance. However, the rain rate statistics given by ITU-R P  
281 837-6 seems quite larger compared with the results from EU NIMROD data interpolate from 5 km to 1 km and estimated  
282 directly for 1 km data. This suggests that the ITU. Rec tends to over-estimates rain. Indeed, the overestimation of ITU-R P.837-  
283 6 is likely also due to the overestimation of the rain amounts over oceans as obtained from the ERA-40 data produced by the  
284 ECMWF (i.e. the input maps on which the ITU-R rain rate models relies on). This is why the ITU. Rec recommends users to use  
285 their own data in order to produce better results.

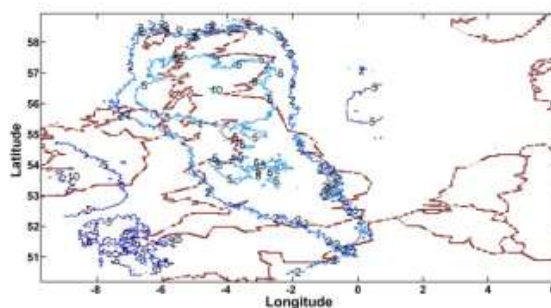


286

287

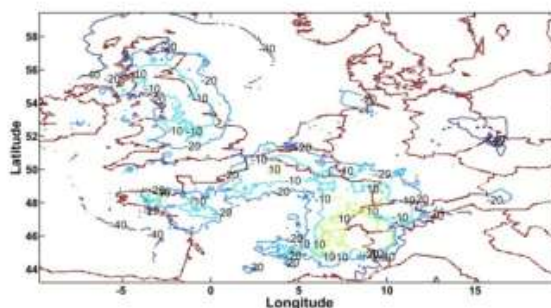
**Figure 8:** Contour map of 0.01% exceeded rain rates of the average year given by ITU-R P 837-6.

288 The differences between EU contour map, UK contour map and ITU contour map have been studied to show how accurate the  
289 proposed approach is. Fig. 9 presents the contour map of the difference of rain rates with 0.01% exceedance based on the EU  
290 data minus UK data. It shows that the proposed approach tends to overestimate the rain rates over land (see the example in  
291 middle area of Fig. 7(b), but under-estimates over the ocean/sea areas (see the left-bottom area of Fig. 7(b)). However, the  
292 difference is acceptable as it is in the range 2 – 5 mm/h for most areas. For some areas, the difference can up to 10 mm/h or  
293 higher, but this is rare.



294

295 **Figure 9:** Contour map of 0.01% exceeded rain rates difference between the prediction from proposed approach and the  
296 measurements from 1 km UK NIMROD.



297

298 **Figure 10:** Contour map of 0.01% exceeded rain rates difference between the prediction from proposed approach and ITU-R P  
299 837-6.

300 Fig. 10 presents the difference between the prediction from the proposed approach and ITU-R P 837-6 (EU predicted rain rates  
301 minus ITU predicted rain rates). The contour map shows that the ITU-R P 837-6 tends to over-estimate rain rate compare to the  
302 proposed approach for most areas. The difference can up to 40 mm/h for some regions. This indicates that the proposed



303 approach gives more plausible estimates than ITU-R P 837-6, although it is restricted to Western Europe. However, it is  
 304 necessary to highlight that for the Grand Massive alpine area of France, the proposed approach gives larger rain rates exceedance  
 305 than ITU-R P 837-6. This indicates that it is hard to give accurate rainfall rate measurements or prediction over mountain area  
 306 due to the difficulties associated with obtaining accurate rain radar readings (Johansson and Chen, 2003).

307 Fig. 9 and Fig. 10 present the visual comparison of 0.01% exceeded rain rates difference between the prediction from proposed  
 308 approach and the measurements from 1 km UK NIMROD and ITU-R P 837-6. However, the error function can give more  
 309 information to the model performance validation. According to (Paulson et al., 2015 and ITU, 2013), the error function can be  
 310 defined as:

$$311 \quad Error = \left| \ln \left( \frac{R_{measured}}{R_{predicted}} \right) \right| \quad (8)$$

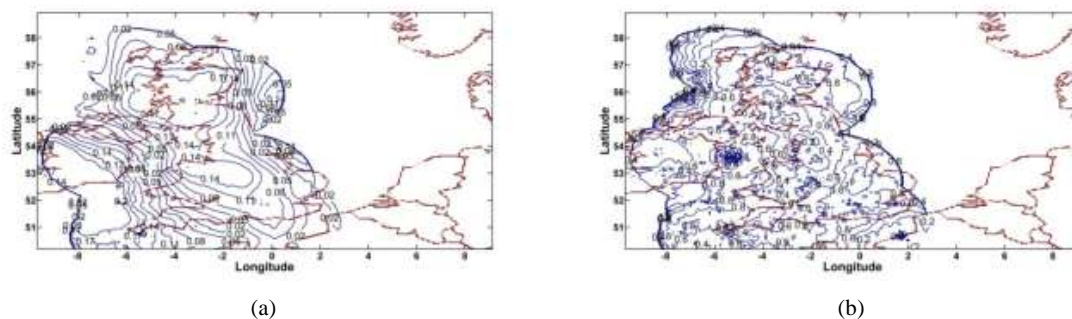
312 where  $R_{measured}$  and  $R_{predicted}$  are the measured and predicted rainfall rate with 0.01% exceedance, respectively. The error at  
 313 each individual location therefore can be calculated by Eq. (8).

314 Fig. 11 shows the error contour maps at 0.01% exceeded rain rate over the UK for both the proposed approach and ITU-Rec  
 315 model. Theoretically, the smaller the error value, the more accurate the model prediction will be. Fig. 11(a) shows that the error  
 316 of the proposed approach is between 0.02 and 0.15. It indicates that the approach proposed in this paper can produce reasonable  
 317 prediction. However, the error from ITU-R model can be up to nearly 2, see Fig. 11(b). Such high error value suggests that it is  
 318 better to use the local rain radar measurements for the model development if the data is available.

319 The mean error  $\overline{Error}$  is calculated by:

$$320 \quad \overline{Error} = \frac{1}{n} \sum_{i=1}^n Error_i \quad (9)$$

321 where  $Error_i$  is the error for individual location and  $n$  is the location index. The  $\overline{Error}$  for ITU-R model is 0.62. It is roughly 7  
 322 times that the proposed approach for which the  $\overline{Error}$  is as low as 0.09.  
 323



324  
 325 (a) (b)  
 326 **Figure 11:** Contour map of error at 0.01% exceeded rain rate: (a) error distribution of proposed model, and (b) error distribution  
 327 of ITU-R P 837-6.

328 **Table 2:** RMSE of lognormal rain distribution parameters  $\{\mu, \sigma\}$  in both space and time domains at four locations.

Portsmouth		Paris	Rennes	Reims	Brussels	Zurich
$\mu$	0.0761	0.0632	0.0945	0.0368	0.0526	0.0875
$\sigma$	0.0485	0.0418	0.0323	0.0477	0.0392	0.0417

329  
 330 In particular, the Root-Mean-Squared Error (RMSE) has been applied to measure the goodness of fit between measured  
 331 lognormal parameter  $\{\mu, \sigma\}$  obtained from radar-derived statistics and predicted  $\mu$  values. The RMSE is defined as



$$332 \quad E = \sqrt{\frac{\sum_1^n (P_v - M_v)^2}{n}} \quad (10)$$

333 where,  $P_v$  and  $M_v$  are predicted and measured values, respectively, and  $n$  represents the number of samples. Table 2 gives the  
334 calculated RMSE of lognormal rain distribution parameters  $\{\mu, \sigma\}$  at six locations cover different climates within the studied  
335 area. The small RMSE (less than 0.1) suggests that the proposed algorithm yields accurate predictions, especially for  $\sigma$ .  
336

### 337 6. Conclusion

338 A simple but efficient interpolation/extrapolation approach has been presented. Instead of the radar-/raingauge-derived rainfall  
339 rate data, the analyzed rain characteristics and fitted coefficients are used to predict rain at many space-time resolutions.  
340 Databases with estimated parameter values, and maps for Europe, have been created to allow users to access the key rain  
341 characteristics at any location within the study area. This provides great assistance to users as the rain characteristics can be  
342 easily obtained without long computation. In particular, an approach to interpolate the fitted coefficients and/or rain  
343 characteristics in space-time domain with arbitrary integration length has been proposed. Although parameters can be estimated  
344 at any combination of spatial and temporal integration lengths by interpolation or/and extrapolation, the results have only been  
345 tested down to 1 km spatial. The predictions have been validated through comparing with the measurements from UK NIMROD  
346 data. The results show that there is a reasonable agreement between the predicted and computed values. However, the predictions  
347 with resolution finer than  $\{1 \text{ km}, 5 \text{ mins}\}$  cannot be validated due to lack of radar/raingauge data.  
348 Finally, the contour map of 0.01% exceeded rain rates cross Western Europe and the British Isles have been generated and  
349 compared using the data interpolated from 5 km to 1 km and estimated directly from 1 km data. The results are also compared  
350 with ITU-R P 837-6 estimations.

### 351 ACKNOWLEDGMENT

352 The authors thank the British Atmospheric Data Centre (BADC), which is part of the NERC National Centre for Atmospheric  
353 Science (NCAS), and the British Met Office for providing access to the NIMROD rain radar data sets (<http://badc.nerc.ac.uk/>).  
354 Partial support from ICT COST action IC0802, "Propagation tools and data for integrated telecommunication, Navigation and  
355 earth observation systems" is gratefully acknowledged.  
356

### 357 Appendix A: Calibration of NIMROD data

358 The calibration of NIMROD data is significant for this study. By choosing some samples (normally the more samples that are  
359 chosen the more accurate the result will be, here the author use 30 samples), two algebraic equations are used, one is for latitude  
360 and the other one is for the longitude. These two numerical equations could allocate the roughly latitude and longitude values for  
361 different locations of Western Europe.

362 For the development of the relative algebraic equations, the general procedures are summarised as following steps:

363 1. Choosing some radar images from NIMROD data set

364 The NIMROD radar-derived rain maps are helpful and critical for the calibration therefore some maps should be selected at the  
365 initial stage. The maps need to meet the following requirements.

- 366 i) There is not too much rain in the selected map, the less the better. Under this circumstance, it could be easier to find some  
367 small rainy areas or even single rain point (ideal situation) from the map. In this way the error can be greatly reduced.
- 368 ii) The separation of different rainy areas in the same map should be large enough; otherwise, it is easy to make a mistake when  
369 trying to find out the corresponding coordinate (row and column) in the grid.



370 2. Allocating the selected samples

371 This piece of work used a map of the Europe (not the NIMROD radar map) that has accurate latitude and longitude information.  
 372 As to the scale, ideally, is the finer the better. Based on this an accurate result can be achieved. In this study, the finest precision  
 373 of the European map used to provide the latitude and longitude information is 20 mins. Through comparing the radar images  
 374 and the used map, the locations of the selected samples can be physically allocated on the map. In addition, both the latitude and  
 375 longitude values of the location of interest can be read and recorded as it is visible on the map.

376 The achieved latitude and longitude values of all selected locations can be transformed into degrees by using the following  
 377 mathematical equation:

$$378 \text{ Finalvalue} = X + \frac{Y}{60} + \frac{Z}{3600} \quad (\text{A1})$$

379 3. Fitting the line

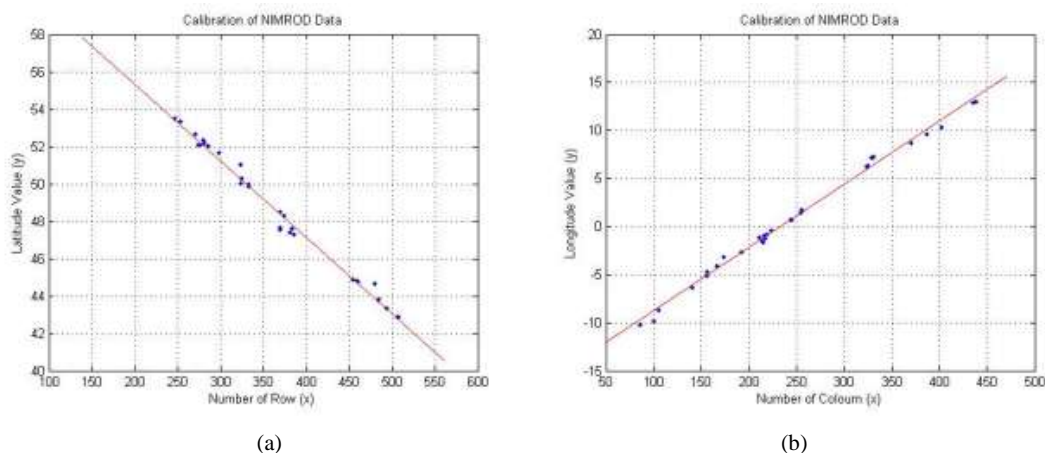
380 It is difficult to get the real latitude and longitude value for the location of interest since error is unavoidable. However, by  
 381 making use of the achieved data from the selected samples, a reasonable line to offset and reduce the error can be proposed.

382 The final equations are given as follows:

$$383 y(\text{longitude}) = 0.0658x - 19.8364 \quad (\text{A2})$$

$$384 y(\text{latitude}) = -0.0409x + 59.430 \quad (\text{A3})$$

385 Here  $x$  denotes either row or column number of the NIMROD data grid with spatial integration length of 5 km, and  $y$  is the  
 386 corresponding coordinate value in either latitude or longitude. The fitted lines are shown in Fig. A.  
 387



388

389

390 **Figure A:** (a) tendency of latitude changing with distance, (b) tendency of longitude changing with distance.

391 Viewed from the software generated figure (see Fig. A), it is clear that the fitted lines are straight. Fig. A(a) shows that the slope  
 392 for the latitude is negative. The reason is that the origin of the data matrix for rain field image is starts from the top left to bottom  
 393 right. It means that the smaller the row number (the value of  $x$ ), the higher the latitude value. In other words, the latitude value  
 394 decreases with the increasing row number. Fig. A(b) shows that the slope for the longitude is positive. Noticeably, the larger the  
 395 column number (the value of  $x$ ), the higher the longitude value. Here, it is important to highlight that the longitude values can be  
 396 either positive or negative. The reason is that the Prime Meridian goes across the studied map.

397

398 **Appendix B: Code for extrapolating the measured data**



```
function Zi=SpaceTime_Interpolation(Data,ZI)
GG = zeros(length(Data),length(Data));
for i = 1 : length(Data)
    for j = 1 : length(Data)
        if i ~= j
            magx = sqrt((Lat(i)-Lat(j))^2 + (Lon(i)-Lon(j))^2);
            if magx >= 1e-7
                GG(i,j) = (magx^2) * (log(magx)-1);
            end
        end
    end
end
m = GG\Z; % Compute model "m" where data "d" is equal to "Z"
% Find 2D interpolated surface through irregular/regular grid points
gg = zeros(size(m));
for i = 1 : size(ZI,1)
    for j = 1 : size(ZI,2)
        for k = 1 : length(Data)
            magx = sqrt((YI(i,j)-Lat(k))^2 + (XI(i,j)-Lon(k))^2);
            if magx >= 1e-7
                gg(k) = (magx^2) * (log(magx)-1);
            end
        end
        ZI(i,j) = sum(gg.*m);
    end
end
for n=1:30
    ZI(Lat(n),Lon(n))=Sample(n);
end
% Plot result if running example or if no output arguments are found
mesh(YI,XI,ZI)
Zi=ZI; % Zi includes all the extropolated data that forms the 3D surface
```

399

## 400 References

- 401 Bell, T. L.: A space-time stochastic model of rainfall for satellite remote-sensing studies. *Journal of Geophysical Research: Atmospheres*, Vol.  
402 92, D8, 9631-9643, 1987.
- 403 Crane, R. K.: *Electromagnetic wave propagation through rain*. Wiley-Interscience, 1996.
- 404 Cowpertwait, P. S.: A spatial-temporal point process model of rainfall for the Thames catchment, UK. *Journal of Hydrology*, 330(3), 586-595,  
405 2006.
- 406 Deidda, R.: Multifractal analysis and simulation of rainfall fields in space. *Physics and Chemistry of the Earth, Part B: Hydrology, Oceans and*  
407 *Atmosphere*, 24(1), 73-78, 1999.
- 408 Deidda, R., Et al.: Multifractal modeling of anomalous scaling laws in rainfall. *Water Resource Research*, Vol. 35, No. 6, 1853-1867, 1999.
- 409 Deidda, R.: Rainfall downscaling in a space-time multifractal framework. *Water Resources Research*, 36(7), 1779-1794, 2000.
- 410 Deidda, R., Et al. Space-time multifractality of remotely sensed rainfall fields. *Journal of hydrology*, 322(1), 2-13, 2006.
- 411 Drozdov, O. A., and Shepelevskii, A. A.: The theory of interpolation in a stochastic field of meteorological elements and its application to met-  
412 eorological maps and network rationalization problems. *Trudy NIU GUGMS*, 1(18), 1946.
- 413 Filip, M. and Vilar, E.: Optimum utilization of the channel capacity of a satellite link in the presence of amplitude scintillations and rain attenu-  
414 ation. *IEEE Transactions on Communications*, 38(11), 1958-1965, 1990.
- 415 Gremont, B., Et al.: Comparative analysis and performance of two predictive fade detection schemes for Ka-band fade countermeasures. *IEEE*  
416 *Journal on Communications*, 17(2), 180-192, 1999.
- 417 Guillot, G. and Lebel, T.: Disaggregation of Sahelian mesoscale convective system rain fields: Further developments and validation. *Journal of*  
418 *Geophysical Research: Atmospheres* (1984–2012), 104(D24), 31533-31551, 1999.
- 419 Hubert, P., Et al.: Multifractals and extreme rainfall events. *Geophysical Research Letters*, 20(10), 931-934, 1993.
- 420 International Telecommunication Union (ITU): Characteristics of precipitation for propagation modelling. ITU-R Recomm. P. 837-6, Geneva,  
421 2013.
- 422 International Telecommunication Union (ITU): Acquisition, presentation and analysis of data in studies of tropospheric propagation. ITU-R  
423 Recomm. P. 311-14, Geneva, Switzerland, 2013.



- 424 Jeannin, N., Et al.: Statistical distribution of the fractional area affected by rain. *Journal of Geophysical Research: Atmospheres*, Vol. 113, D21,  
425 2008.
- 426 Jeannin, N., Et al.: A large-scale space-time stochastic simulation tool of rain attenuation for the design and optimization of adaptive satellite  
427 communication systems operating between 10 and 50 GHz. *International Journal of Antennas and Propagation*, 2012.
- 428 Johansson, B. and Chen, D.: The influence of wind and topography on precipitation distribution in Sweden: Statistical analysis and modelling.  
429 *International Journal of Climatology*, 23(12), 1523-1535, 2003.
- 430 Keys, R. G.: Cubic convolution interpolation for digital image processing. *Acoustics, Speech and Signal Processing, IEEE Transactions*, 29(6),  
431 1153-1160, 1981.
- 432 Kiely, G., and Ivanova, K.: Multifractal analysis of hourly precipitation. *Physics and Chemistry of the Earth, Part B: Hydrology, Oceans and At-*  
433 *mosphere*, 24(7), 781-786, 1999.
- 434 Kundu, P. K. and Bell, T. L.: Space-time scaling behavior of rain statistics in a stochastic fractional diffusion model. *Journal of Hydrology*, 32-  
435 2(1), 49-58, 2006.
- 436 Lovejoy, S. and Mandelbrot, B. B.: Fractal properties of rain, and a fractal model. *Tellus, Series A- Dynamic Meteorology and Oceanography*,  
437 37, 209-232, 1985.
- 438 Luini, L. and Capsoni, C.: MultiEXCELL: a new rain field model for propagation applications. *IEEE Transactions on Antennas and Propagati-*  
439 *on*, 59(11), 4286-4300, 2011.
- 440 Mandelbrot, B. B.: How long is the coast of Britain. *Science*, 156(3775), 636-638, 1967.
- 441 Matheron, G.: The theory of regional characterising sed Variables and Its Applications. *Cahiers du Centre de Morphologie Mathematique, Eco-*  
442 *le des Mines, Fountainbleau, France*, 211, 1971.
- 443 Menabde, M., Et al.: Self-similar random fields and rainfall simulation. *Journal of Geophysical Research: Atmospheres*. Vol. 102, D12, 13509-  
444 13515, 1997.
- 445 Menabde, M., Et al.: Self-similar random fields and rainfall simulation. *Journal of Geophysical Research: Atmospheres*, Vol. 102, D12, 13509-  
446 13515, 1997.
- 447 Olsson, J. and Niemczynowicz, J.: Multifractal analysis of daily spatial rainfall distributions. *Journal of Hydrology*, 187(1), 29-43, 1996.
- 448 Olsson, J., Et al.: Fractal analysis of high-resolution rainfall time series. *Journal of Geophysical Research Atmospheres*, Vol. 98, D12, 23265-  
449 23274, 1993.
- 450 Olsson, J.: Evaluation of a scaling cascade model for temporal rain-fall disaggregation. *Hydrology and Earth System Sciences Discussions, Eu-*  
451 *ropean Geosciences Union*, 2(1), 19-30, 1998.
- 452 Pathirana, A., Et al.: Estimating rainfall distributions at high temporal resolutions using a multifractal model. *Hydrology and Earth System Sci-*  
453 *Paulson, K. S.: Fractal interpolation of rain rate time series. Journal of Geophysical Research: Atmospheres (1984–2012)*, 109(D22), 2004.
- 454 Paulson, K. S., Et al.: A method to estimate trends in distributions of 1 min rain rates from numerical weather prediction data. *Radio Science*,  
455 50.9: 931-940, 2015.
- 456 Reborá, N., Et al.: RainFARM: Rainfall downscaling by a filtered autoregressive model. *Journal of Hydrometeorology*, 7(4), 724-738, 2006.
- 457 Svensson, C., Et al.: Multifractal properties of daily rainfall in two different climates. *Water Resources Research*, 32(8), 2463-2472, 1996.
- 458 Taylor, G. I.: The spectrum of turbulence. In *Proceedings of the Royal Society of London A: Mathematical, Physical and Engineering Sciences*,  
459 Vol. 164, issue 919, 476-490, Feb 1938.
- 460 Veneziano, D., Et al.: Nonlinearity and self-similarity of rainfall in time and a stochastic model. *Journal of Geophysical Research: Atmospheres*  
461 Vol. 101, D21, 26371-26392, 1996.
- 462 Venugopal, V., Et al.: A space-time downscaling model for rainfall. *Journal of Geophysical Research*, 104(D4), 19705-19721, 1999.
- 463 Venugopal, V., Et al.: Evidence of dynamic scaling in space-time rainfall. *Journal of Geophysical Research: Atmospheres*, 104(D24), 31599-  
464 31610, 1999.
- 465 Voss, R. F.: Random fractal forgeries. In *Fundamental algorithms for computer graphics*, 805-835. Springer Berlin Heidelberg, 1985.
- 466 *ences Discussions*, 7(5), 668-679, 2003.
- 467 Yaglom, A. M.: The influence of fluctuations in energy dissipation on the shape of turbulence characteristics in the inertial interval. In *Soviet*



468 Physics Doklady, 11, 26, Jul 1966.

469 Yang, G.: Rainfall Rate Modelling For European Satellite Networks. PhD thesis, University of Portsmouth, 2016.

470 Yang, G., Et al.: Characterization of rain fields for UK satellite networks. In Ka and Broadband Communications: navigation and Earth observ-

471 ation conference, Oct 2011.